European Journal of Mechanics / B Fluids 94 (2022) 121–127

Contents lists available at ScienceDirect

European Journal of Mechanics / B Fluids

journal homepage: www.elsevier.com/locate/ejmflu

Multiple solutions of the unsteady hybrid nanofluid flow over a rotating disk with stability analysis

Iskandar Waini [a,b], Anuar Ishak [b], Ioan Pop [c,*]

[a] Fakulti Teknologi Kejuruteraan Mekanikal dan Pembuatan, Universiti Teknikal Malaysia Melaka, Hang Tuah Jaya, 76100 Durian Tunggal, Melaka, Malaysia
[b] Department of Mathematical Sciences, Faculty of Science and Technology, Universiti Kebangsaan Malaysia, 43600 UKM Bangi, Selangor, Malaysia
[c] Department of Mathematics, Babeş-Bolyai University, 400084 Cluj-Napoca, Romania

ARTICLE INFO

Article history:
Received 28 August 2021
Received in revised form 29 December 2021
Accepted 23 February 2022
Available online 4 March 2022

Keywords:
Hybrid nanofluid
Unsteady flow
Heat transfer
Rotating disk
Multiple solutions
Stability analysis

ABSTRACT

The present study attempts to analyze the unsteady flow over a rotating disk in a hybrid nanofluid with suction and deceleration effects. The partial derivatives of multivariable differential equations are converted to ordinary differential equations using appropriate transformations. The bvp4c function in MATLAB software is employed to solve the mathematical model. The outcomes show that multiple solutions are verifiable in certain operating parameters. The stability of the multiple solutions over time is investigated. It is discovered that the first and the second solutions are stable and physically relevant, whereas the third solution is unstable as time evolves. Moreover, the stronger deceleration contributes to enhancing the skin friction coefficient in the radial direction $\mathrm{Re}_r^{1/2}C_f$ and in the azimuthal direction $\mathrm{Re}_r^{1/2}C_g$, for the first and third solutions whereas the second solution reduces. The values of $\mathrm{Re}_r^{1/2}C_f$ and $\mathrm{Re}_r^{1/2}C_g$ for the third solution enhance in the presence of suction, while the opposite behaviors are observed for the first and second solutions. The enhancement of the local Nusselt number $\mathrm{Re}_r^{-1/2}Nu_r$ on all solutions is noticed with the imposition of suction on the surface and stronger deceleration strength.

1. Introduction

Fluid flow and heat transfer issues are critical to the design and optimization of a high-efficiency system [1]. Scientists and engineers have therefore evolved an upgraded thermal fluid with the addition of nano-sized solid particles to the base fluid established by Choi and Eastman [2]. These mixtures are called "nanofluids" and are believed to improve the thermal conductivity of the base fluid. The benefits of the use of rectangular enclosure-filled nanofluids have been assessed by several researchers, see Refs. [3–5]. Besides, several researchers have published papers on nanofluids with various physical aspects, for example, the magnetic field effects [6,7], the viscous dissipation [8,9], the chemical reaction and the activation energy effects [10–12], the mixed convection effects [13,14], the Dufour and Soret effects [15,16], and the Joule heating effects [17,18]. Also, the nanofluid flow over a rotating disk and inside an asymmetric wavy channel were studied by Ellahi et al. [19,20], respectively. Moreover, Turkyilmazoglu [21,22] examined the nanofluid flow past an impulsive vertical plate and moving inclined substrate, respectively.

The nanofluid idea was extended to two or more nanoparticles simultaneously scattered into the base fluid and named it as 'hybrid nanofluid'. Hybrid nanofluid is utilized to signal a promising increase in the thermal performance of working fluids since this technology has resulted in a significant change in the design of thermal and cooling systems. As a result of the addition of more types of nanostructures, a fluid with better thermal conductivity is created. Hybrid nanofluid is used in several applications, for example, vehicle brake fluid, solar water heating, domestic refrigerator, heat exchanger, and transformer [23]. The prior experimental works using the hybrid nanoparticles have been done by several researchers, see Refs. [24,25]. The thermal conductivity of Cu-Al_2O_3/water hybrid nanofluid has been experimentally studied by Suresh et al. [26]. They stated that, although Al_2O_3 has low thermal conductivity, there is a good chemical inertness in alumina that could maintain the stability of the hybrid nanofluid. Besides, the significance of the combination of Al_2O_3 and other nanoparticles was reported by Singh and Sarkar [27] and Farhana et al. [28]. Furthermore, the thermophysical developed by Takabi and Salehi [29] showed a remarkable comparison with the experiment data. The topic of hybrid nanofluid has attracted researchers to conduct the theoretical study, for example, Jamaludin et al. [30], Khan et al. [31], Khashi'ie et al. [32], Zainal et al. [33], Waini et al. [34–36], Hassan et al. [37], and Riaz et al.

* Corresponding author.
E-mail address: popm.ioan@yahoo.co.uk (I. Pop).

https://doi.org/10.1016/j.euromechflu.2022.02.011
0997-7546/

[38]. Moreover, readers may read the following review papers on hybrid nanofluids for further overview, see Refs. [39–42].

The infinite rotating disk in a steady viscous flow was pioneered by Von Kármán [43] where the disk rotates with the uniform angular velocity. The author employed the similarity variables which allowed the Navier–Stokes equations reduce to ordinary differential equations. The centrifuge effect surrounding the disk creates a radially outbound flow, to which a vertical downbound move towards the disk compensates. Von Kármán's work has resulted in some research papers published in this area. Fang [44] investigated the flow on a stretchable rotating disk, while Fang and Zhang [45] later examined the flow between two infinite stretchable disks. The work of Fang [12] was extended by Turkyilmazoglu [46] by considering the magnetic field with the viscous dissipation and the joule heating effects in the energy equation. Turkyilmazoglu [47] has also considered the magnetohydrodynamic flow due to a porous rotating disk subject to a uniform outer radial flow, while the unsteady flow over a decelerating rotating sphere was reported by Turkyilmazoglu [48]. Moreover, Watson and Wang [49] originally examined the unsteady flow on a rotating disk. The disk angular velocity was inverted proportional to time and the similarity equations were determined. The authors have shown that the solution exists only on the decelerated rotating disks. This deceleration disk problem has been further extended to porous disks, which include the effects of mass transfer by Watson et al. [50]. Later, Fang and Tao [51] considered the unsteady viscous flow due to the rotating stretching disk. Then, several kinds of research on rotating disks have been considered by the researchers with various physical aspects. For example, Naganthran et al. [52] considered the shrinking disk with the variable fluid properties, Sarkar and Sahoo [53] studied the magnetic field effects, and the effects of the nanoparticles were examined by Rafiq and Mustafa [54]. The theoretical studies of fluid flow due to rotating disks have gotten a lot of attention from researchers and scientists because of their numerous applications in industries and engineering, such as viscometers, turbines, rotating disk electrodes, spin-coating, centrifugal pumps, fans, and rotors [53,54].

The present study considers the unsteady flow over a rotating disk containing Cu-Al_2O_3/water hybrid nanofluid with the suction and the deceleration effects. Most importantly, multiple solutions are obtained for certain pertinent parameters, and the stability of the solutions is also reported in this study. The outcomes are original and not yet available in the literature and therefore, this endeavor is significant as a future reference for the selected topic.

2. Mathematical model

Consider the unsteady hybrid nanofluid flow over a rotating permeable stretching disk as illustrated in Fig. 1. The disk is stretched with the velocity, $u = u_w$ and rotates with the velocity, $v = v_w$. Besides, the mass flux velocity, $w = w_w$ is considered to represent the permeability of the disk. Also, the surface and ambient temperatures are assumed constants and are denoted by T_w and T_∞, respectively. Thus, the governing equations can be written in cylindrical coordinates as follows [51,54]:

$$\frac{\partial}{\partial r}(ru) + \frac{\partial}{\partial z}(rw) = 0 \tag{1}$$

$$\frac{\partial u}{\partial t} + u\frac{\partial u}{\partial r} + w\frac{\partial u}{\partial r} - \frac{v^2}{r} = -\frac{1}{\rho_{hnf}}\frac{\partial p}{\partial r} + \frac{\mu_{hnf}}{\rho_{hnf}}\left(\frac{\partial^2 u}{\partial r^2} + \frac{1}{r}\frac{\partial u}{\partial r} + \frac{\partial^2 u}{\partial z^2} - \frac{u}{r^2}\right) \tag{2}$$

$$\frac{\partial v}{\partial t} + u\frac{\partial v}{\partial r} + w\frac{\partial v}{\partial z} + \frac{uv}{r} = \frac{\mu_{hnf}}{\rho_{hnf}}\left(\frac{\partial^2 v}{\partial r^2} + \frac{1}{r}\frac{\partial v}{\partial r} + \frac{\partial^2 v}{\partial z^2} - \frac{v}{r^2}\right) \tag{3}$$

Table 1
Thermophysical properties [5].

Properties	Nanoparticles		Base fluid
	Cu	Al_2O_3	water
ρ (kg/m^3)	8933	3970	997.1
C_p (J/kgK)	385	765	4179
k (W/mK)	400	40	0.613
Prandtl number, Pr			6.2

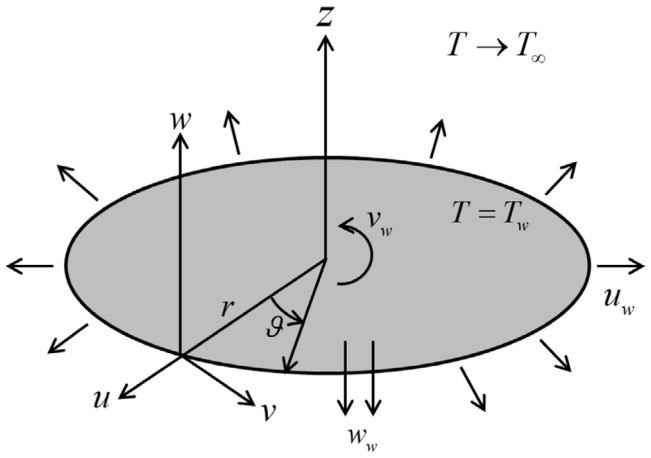

Fig. 1. Physical model.

$$\frac{\partial w}{\partial t} + u\frac{\partial w}{\partial r} + w\frac{\partial w}{\partial z} = -\frac{1}{\rho_{hnf}}\frac{\partial p}{\partial z} + \frac{\mu_{hnf}}{\rho_{hnf}}\left(\frac{\partial^2 w}{\partial r^2} + \frac{1}{r}\frac{\partial w}{\partial r} + \frac{\partial^2 w}{\partial z^2}\right) \tag{4}$$

$$\frac{\partial T}{\partial t} + u\frac{\partial T}{\partial r} + w\frac{\partial T}{\partial z} = \frac{k_{hnf}}{(\rho C_p)_{hnf}}\left(\frac{\partial^2 T}{\partial r^2} + \frac{1}{r}\frac{\partial T}{\partial r} + \frac{\partial^2 T}{\partial z^2}\right) \tag{5}$$

subject to:

$$\begin{aligned} &u = \lambda u_w, \quad v = v_w, \quad w = w_w, \quad T = T_w \quad \text{at} \quad z = 0 \\ &u \to 0, \quad v \to 0, \quad w \to 0, \quad T \to T_\infty \quad \text{as} \quad z \to \infty \end{aligned} \tag{6}$$

where (u, v, w) are the respective velocity components along (r, ϑ, z) directions, and T denotes the fluid temperature. To obtain the similarity equations, it is assumed that $u_w = \Omega r/(1-ct)$ and $v_w = \Omega r/(1-ct)$ where t is the time, Ω is the constant angular velocity, and c is the constant showing the unsteadiness strength. Besides, $w_w = -w_0/\sqrt{1-ct}$ where w_0 is a constant. Also, λ is the stretching parameter where $\lambda = 0$ is for a static disk and $\lambda > 0$ corresponds to the stretching disk.

Further, the thermophysical properties of the base fluid (water), Al_2O_3, and Cu nanoparticles are provided in Table 1 [5]. The hybrid nanofluid correlations are given in Eq. (7), as follows, [29]:

$$\begin{aligned} &\rho_{hnf} = (1-\varphi_{hnf})\rho_f + \varphi_1\rho_{n1} + \varphi_2\rho_{n2}, \quad \mu_{hnf} = \frac{\mu_f}{(1-\varphi_{hnf})^{2.5}}, \\ &(\rho C_p)_{hnf} = (1-\varphi_{hnf})(\rho C_p)_f + \varphi_1(\rho C_p)_{n1} + \varphi_2(\rho C_p)_{n2}, \\ &\frac{k_{hnf}}{k_f} = \frac{\frac{\varphi_1 k_{n1} + \varphi_2 k_{n2}}{\varphi_{hnf}} + 2k_f + 2(\varphi_1 k_{n1} + \varphi_2 k_{n2}) - 2\varphi_{hnf}k_f}{\frac{\varphi_1 k_{n1} + \varphi_2 k_{n2}}{\varphi_{hnf}} + 2k_f - (\varphi_1 k_{n1} + \varphi_2 k_{n2}) + \varphi_{hnf}k_f} \end{aligned} \tag{7}$$

with the density ρ_{hnf}, the dynamic viscosity μ_{hnf}, the heat capacitance $(\rho C_p)_{hnf}$, and the thermal conductivity k_{hnf}. Note that, Al_2O_3 and Cu nanoparticles are given by φ_1 and φ_2, respectively, with

$\varphi_{hnf} = \varphi_1 + \varphi_2$. Besides, the subscripts $n1$ and $n2$ denote their solid components.

Now, consider the following similarity transformations [51,54]:

$$u = \frac{\Omega r}{1-ct} f'(\eta), \quad v = \frac{\Omega r}{1-ct} g(\eta), \quad w = -\frac{2\sqrt{\Omega \nu_f}}{\sqrt{1-ct}} f(\eta),$$
$$\theta(\eta) = \frac{T - T_\infty}{T_w - T_\infty}, \quad \eta = \sqrt{\frac{\Omega}{\nu_f}} \frac{z}{\sqrt{1-ct}} \tag{8}$$

where prime denotes differentiation with respect to η. On using (8), Eq. (1) is fully satisfied. Then, Eqs. (2)–(5) becomes:

$$\frac{\mu_{hnf}/\mu_f}{\rho_{hnf}/\rho_f} f''' + 2ff'' - f'^2 + g^2 - S\left(f' + \frac{1}{2}\eta f''\right) = 0 \tag{9}$$

$$\frac{\mu_{hnf}/\mu_f}{\rho_{hnf}/\rho_f} g'' + 2fg' - 2f'g - S\left(g + \frac{1}{2}\eta g'\right) = 0 \tag{10}$$

$$\frac{1}{\Pr} \frac{k_{hnf}/k_f}{\left(\rho C_p\right)_{hnf} / \left(\rho C_p\right)_f} \theta'' + 2f\theta' - \frac{1}{2} S\eta\theta' = 0 \tag{11}$$

subject to:

$$f(0) = \frac{B}{2}, \quad f'(0) = \lambda, \quad g(0) = 1, \quad \theta(0) = 1;$$
$$f'(\eta) \to 0, \quad g(\eta) \to 0, \quad \theta(\eta) \to 0 \quad \text{as} \quad \eta \to \infty \tag{12}$$

In Eqs. (9)–(12), $S = c/\Omega$ is the unsteadiness parameter with $S < 0$ indicates the deceleration of the disk, $\Pr = \left(\mu C_p\right)_f / k_f$ is the Prandtl number, and $B = w_0/\sqrt{\Omega \nu_f}$ is the mass flux parameter with $B > 0$ is for the suction case.

The physical quantities of interest are the skin friction coefficients on the radial C_f and the azimuthal C_g directions, and the local Nusselt number Nu_r, which are defined as:

$$C_f = \frac{\mu_{hnf}}{\rho_f u_w^2} \left(\frac{\partial u}{\partial z}\right)_{z=0}, \quad C_g = \frac{\mu_{hnf}}{\rho_f v_w^2} \left(\frac{\partial v}{\partial z}\right)_{z=0},$$
$$Nu_r = -\frac{r k_{hnf}}{k_f (T_w - T_\infty)} \left(\frac{\partial T}{\partial z}\right)_{z=0} \tag{13}$$

Using (8) and (13), one gets:

$$\mathrm{Re}_r^{1/2} C_f = \frac{\mu_{hnf}}{\mu_f} f''(0), \quad \mathrm{Re}_r^{1/2} C_g = \frac{\mu_{hnf}}{\mu_f} g'(0),$$
$$\mathrm{Re}_r^{-1/2} Nu_r = -\frac{k_{hnf}}{k_f} \theta'(0) \tag{14}$$

where $\mathrm{Re}_r = u_w r/\nu_f$ is the local Reynolds number.

Note that, for the viscous fluid ($\varphi_1 = \varphi_2 = 0$), Eqs. (9) and (10) reduce to Eqs. (5) and (6) in Fang and Tao [51]. However, the energy equation which is given in Eq. (11) has not been considered by them.

3. Stability analysis

The temporal stability of the solutions is examined by following [55,56]. Firstly, consider the following variables:

$$u = \frac{\Omega r}{1-ct} \frac{\partial f}{\partial \eta}(\eta, \tau), \quad v = \frac{\Omega r}{1-ct} g(\eta, \tau),$$
$$w = -\frac{2\sqrt{\Omega \nu_f}}{\sqrt{1-ct}} f(\eta, \tau),$$
$$\theta(\eta, \tau) = \frac{T - T_\infty}{T_w - T_\infty}, \quad \eta = \sqrt{\frac{\Omega}{\nu_f}} \frac{z}{\sqrt{1-ct}}, \quad \tau = \frac{\Omega r}{1-ct} t \tag{15}$$

where τ is the dimensionless time variable. Then, on using Eq. (15), one obtains:

$$\frac{\mu_{hnf}/\mu_f}{\rho_{hnf}/\rho_f} \frac{\partial^3 f}{\partial \eta^3} + 2f \frac{\partial^2 f}{\partial \eta^2} - \left(\frac{\partial f}{\partial \eta}\right)^2 + g^2 - S\left(\frac{\partial f}{\partial \eta} + \frac{1}{2}\eta \frac{\partial^2 f}{\partial \eta^2}\right)$$
$$- (1 + S\tau) \frac{\partial^2 f}{\partial \eta \partial \eta} = 0 \tag{16}$$

$$\frac{\mu_{hnf}/\mu_f}{\rho_{hnf}/\rho_f} \frac{\partial^2 g}{\partial \eta^2} + 2f \frac{\partial g}{\partial \eta} - 2\frac{\partial f}{\partial \eta} g - S\left(g + \frac{1}{2}\eta \frac{\partial g}{\partial \eta}\right)$$
$$- (1 + S\tau) \frac{\partial^2 g}{\partial \eta \partial \eta} = 0 \tag{17}$$

$$\frac{1}{\Pr} \frac{k_{hnf}/k_f}{\left(\rho C_p\right)_{hnf} / \left(\rho C_p\right)_f} \frac{\partial^2 \theta}{\partial \eta^2} + 2f \frac{\partial \theta}{\partial \eta}$$
$$- \frac{1}{2} S\eta \frac{\partial \theta}{\partial \eta} - (1 + S\tau) \frac{\partial \theta}{\partial \tau} = 0 \tag{18}$$

subject to:

$$f(0, \tau) = \frac{B}{2}, \quad \frac{\partial f}{\partial \eta}(0, \tau) = \lambda, \quad g(0, \tau) = 1, \quad \theta(0, \tau) = 1;$$
$$\frac{\partial f}{\partial \eta}(\eta, \tau) \to 0, \quad g(\eta, \tau) \to 0, \quad \theta(\eta, \tau) \to 0 \quad \text{as} \quad \eta \to \infty \tag{19}$$

Next, consider the perturbation function [56]:

$$f(\eta, \tau) = f_0(\eta) + e^{-\alpha\tau} F(\eta, \tau),$$
$$g(\eta, \tau) = g_0(\eta) + e^{-\alpha\tau} G(\eta, \tau),$$
$$\theta(\eta, \tau) = \theta_0(\eta) + e^{-\alpha\tau} H(\eta, \tau) \tag{20}$$

where $F(\eta, \tau)$, $G(\eta, \tau)$, and $H(\eta, \tau)$ are arbitrary functions and relatively small compared to $f_0(\eta)$, $g_0(\eta)$, and $\theta_0(\eta)$, and α denotes the unknown eigenvalue. Here, Eq. (20) is employed to obtain the eigenvalue problems of Eqs. (16)–(18). By setting $\tau = 0$, then $F(\eta, \tau) = F_0(\eta)$, $G(\eta, \tau) = G_0(\eta)$, and $H(\eta, \tau) = H_0(\eta)$. Therefore, after linearization, the eigenvalue problems are:

$$\frac{\mu_{hnf}/\mu_f}{\rho_{hnf}/\rho_f} F_0''' + 2\left(f_0 F_0'' + f_0'' F_0\right) - 2f_0' F_0' + 2g_0 G_0$$
$$- S\left(F_0' + \frac{1}{2}\eta F_0''\right) + \alpha F_0' = 0 \tag{21}$$

$$\frac{\mu_{hnf}/\mu_f}{\rho_{hnf}/\rho_f} G_0'' + 2\left(f_0 G_0' + g_0' F_0\right) - 2\left(f_0' G_0 + g_0 F_0'\right)$$
$$- S\left(G_0 + \frac{1}{2}\eta G_0'\right) + \alpha G_0 = 0 \tag{22}$$

$$\frac{1}{\Pr} \frac{k_{hnf}/k_f}{\left(\rho C_p\right)_{hnf} / \left(\rho C_p\right)_f} H_0'' + 2\left(f_0 H_0' + \theta_0' F_0\right) - \frac{1}{2} S\eta H' + \alpha H_0 = 0 \tag{23}$$

subject to:

$$F_0(0) = 0, F_0'(0) = 0, G_0(0) = 0, H_0(0) = 0;$$
$$F_0'(\eta) \to 0, G_0(\eta) \to 0, H_0(\eta) \to 0 \text{ as } \eta \to \infty \tag{24}$$

Here, to obtain α from Eqs. (21)–(23), $F_0'(\eta) \to 0$ as $\eta \to \infty$ in Eq. (24) is replaced by $F''(0) = 1$ [57].

4. Results and discussion

This section provides a discussion of the results obtained from the numerical computational. Here, Eqs. (9)–(12) are solved numerically by utilizing the bvp4c solver in MATLAB software. As described in Shampine et al. [58,59], the aforesaid solver occupies a finite difference method that employs the 3-stage Lobatto IIIa formula. The selection of the initial guess and the boundary layer thickness, η_∞ is important to achieve the convergence of the numerical solution. In this respect, we are considering $\eta_\infty = 10$ so that the numerical values obtained are satisfactory,

Table 2
The smallest eigenvalues α for different S when $\lambda = B = 0$, $\varphi_1 = \varphi_2 = 0.01$ and $\mathrm{Pr} = 6.2$.

S	Smallest eigenvalues α		
	First solution	Second solution	Third solution
−2	2.9702	2.5323	−0.9471
−3	4.2140	4.4721	−1.4495
−4	5.2325	6.3055	−2.1532

Table 3
Values of $f''(0)$ and $g'(0)$ for different λ and S when $B = 0$ and $\varphi_1 = \varphi_2 = 0$ (regular fluid).

λ	S	Fang and Tao [51]		Present results	
		$f''(0)$	$g'(0)$	$f''(0)$	$g'(0)$
0	−1	0.7198	−0.2366	0.719787	−0.236575
	−2	0.9315	0.1550	0.931507	0.154981
	−5	1.5627	1.3609	1.562797	1.360850
	−10	2.6008	3.4139	2.600801	3.413860
1	−1	−0.6520	−1.2716	−0.651955	−1.271556
	−2	−0.3517	−1.0534	−0.351741	−1.053409
	−5	0.5632	−0.3882	0.563176	−0.388169
	−10	2.1153	0.7424	2.115331	0.742353

where the infinity boundary conditions are satisfied asymptotically. This convergence issue is also influenced by the values of the considered physical parameters.

Further, the numerical results are then presented in tables and graphical forms. In this study, multiple solutions are obtained, and the existence of these non-unique solutions is possible for the similarity equations and boundary conditions (9) to (12). Therefore, the stability analysis is conducted to address which of the solutions are stable over time and thus reliable in the real-life application. From the relations that are given in Eq. (19), the solutions are stable or physically relevant in the long run when $\alpha > 0$, while $\alpha < 0$ denotes the unstable solution. Table 2 presents the variations of the smallest eigenvalues α for different S when $\lambda = B = 0$, $\varphi_1 = \varphi_2 = 0.01$ and $\mathrm{Pr} = 6.2$. Interestingly, from our calculations, it is shown that the first and the second solutions give the positive values of α, while the negative values of α is obtained for the third solution. Hence, it can be concluded that the first and the second solutions are stable, while the third solution is unstable over time. Although, the first solution and the second solution have stable eigenvalues, the second solution may be physically refuted on the grounds that the flow should rotate in the same direction as the disk, since no external force is applied to reverse the flow swirl direction, see Turkyilmazoglu [47].

The values of $f''(0)$ and $g'(0)$ for different values of λ and S when $B = 0$ and $\varphi_1 = \varphi_2 = 0$ (regular fluid) are given in Table 3. Note that, these physical quantities increase for stronger deceleration ($S < 0$), and their values are greater for the static disk ($\lambda = 0$) compared to the stretching disk ($\lambda = 1$). Besides, the direct comparison is conducted with Fang and Tao [51] and shows a great agreement. It lends trust to the validity and the correctness of the current numerical results. Additionally, Table 4 provides the comparison values of $\mathrm{Re}_r^{1/2}C_g$ and $\mathrm{Re}_r^{-1/2}Nu_r$ for S and B when $\lambda = 0$, $\varphi_1 = 0$, $\varphi_2 = 0.2$ and $\mathrm{Pr} = 6.2$ with Rafiq and Mustafa [54] and the results show an excellent agreement. This is the further evidence that supports the acceptability of the present computation.

Further, Figs. 2–4 are provided to get a clearer insight into the influence of S and B on the variations of $\mathrm{Re}_r^{1/2}C_f$, $\mathrm{Re}_r^{1/2}C_g$, and $\mathrm{Re}_r^{-1/2}Nu_r$. It is worth mentioning that multiple solutions are obtained for this particular problem. These findings are new and not yet reported in the literature. For the fixed values ($\varphi_1 = \varphi_2 = 0.01$, $\lambda = 0$, and $\mathrm{Pr} = 6.2$), it can be seen that stronger deceleration ($S < 0$) gives greater values of $\mathrm{Re}_r^{1/2}C_f$ and

Table 4
Values of $\mathrm{Re}_r^{1/2}C_g$ and $\mathrm{Re}_r^{-1/2}Nu_r$ for S and B when $\lambda = 0$, $\varphi_1 = 0$, $\varphi_2 = 0.2$ and $\mathrm{Pr} = 6.2$.

S	B	Rafiq and Mustafa [54]		Present results	
		$\mathrm{Re}_r^{1/2}C_g$	$\mathrm{Re}_r^{-1/2}Nu_r$	$\mathrm{Re}_r^{1/2}C_g$	$\mathrm{Re}_r^{-1/2}Nu_r$
0	1	− 2.857060	6.124404	−2.856790	6.124492
−1		− 2.171201	6.815980	−2.171200	6.815976
−2		− 1.487684	7.356722	−1.487684	7.356715
−5		0.555397	8.602114	0.555397	8.602102
−1.5	0	− 0.089041	2.679370	−0.089042	2.679362
	1	− 1.829232	7.098926	−1.829232	7.098920
	2	− 4.592431	12.585845	−4.592431	12.585842
	5	− 12.700258	30.176238	−12.700259	30.176237

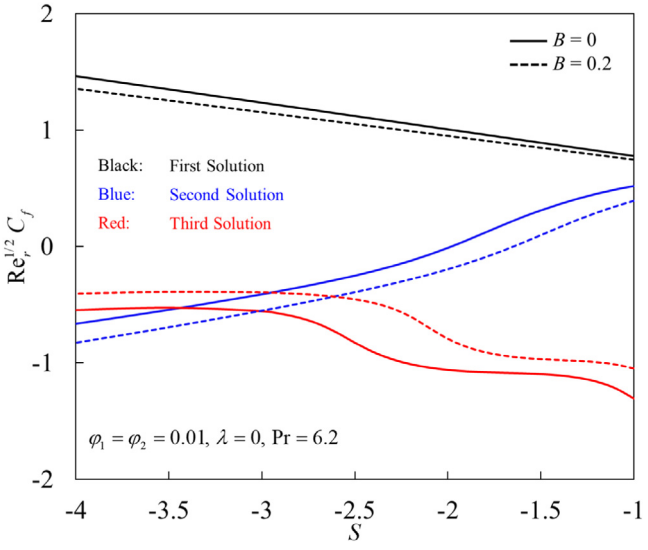

Fig. 2. Skin friction coefficient in the radial direction $\mathrm{Re}_r^{1/2}C_f$ vs S for $B = 0, 0.2$.

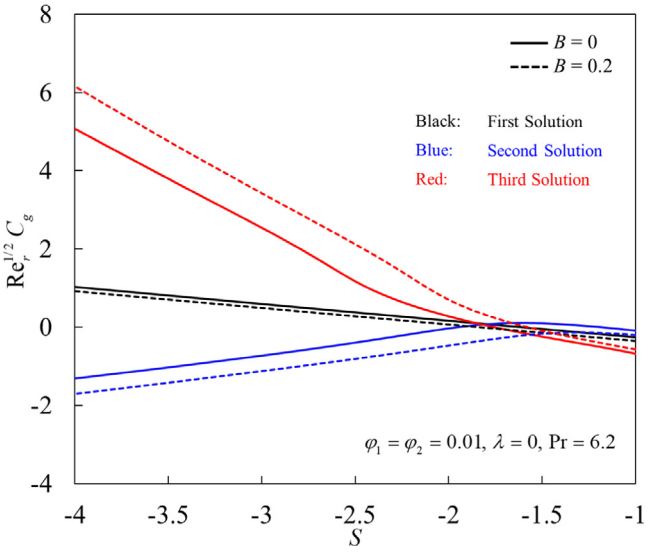

Fig. 3. Skin friction coefficient in the azimuthal direction $\mathrm{Re}_r^{1/2}C_g$ vs S for $B = 0, 0.2$.

$\mathrm{Re}_r^{1/2}C_g$ on the first and third solutions. Physically, this happens due to that resisting force on the disk is boosted by enhancing the deceleration strength. However, the second solution shows quite different behavior where the values of $\mathrm{Re}_r^{1/2}C_f$ and $\mathrm{Re}_r^{1/2}C_g$ decrease. Moreover, the values of $\mathrm{Re}_r^{-1/2}Nu_r$ on all solutions enhance for $S < 0$. Besides, the imposition of suction on the

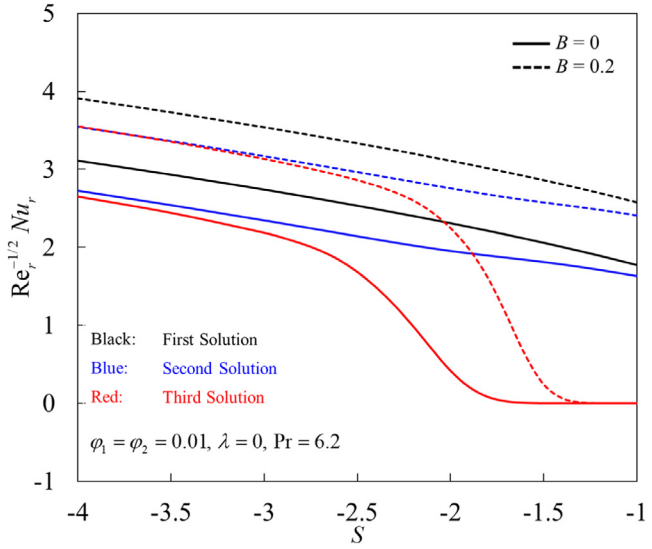

Fig. 4. Local Nusselt number $\mathrm{Re}_r^{-1/2} Nu_r$ vs S for $B = 0, 0.2$.

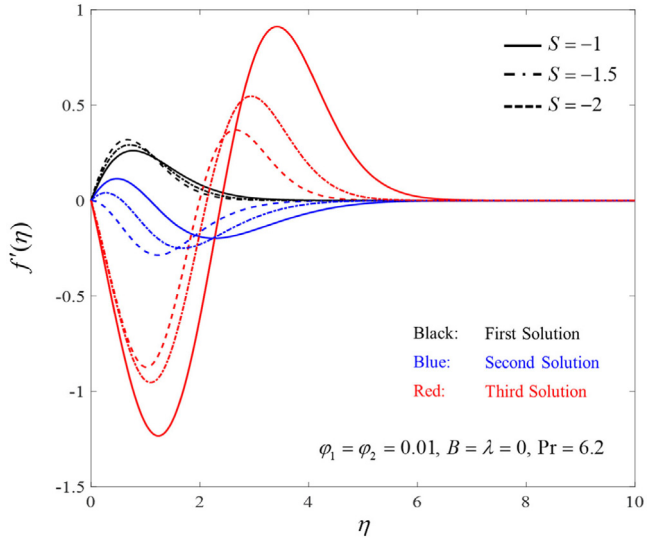

Fig. 5. Radial velocity profiles $f'(\eta)$ vs S.

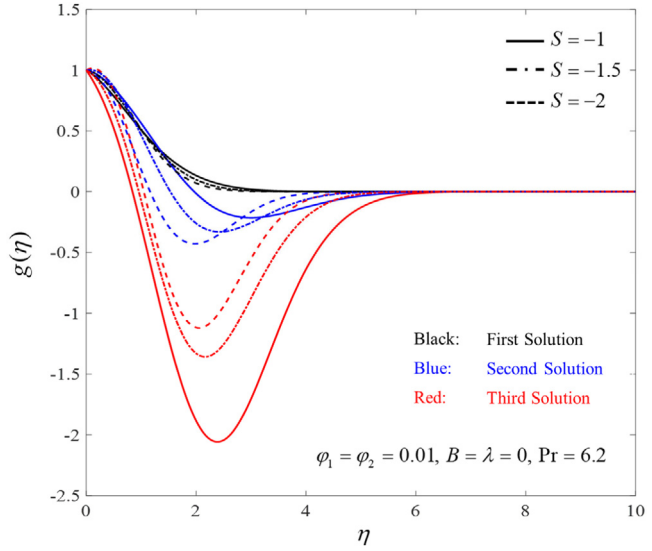

Fig. 6. Azimuthal velocity profiles $g(\eta)$ vs S.

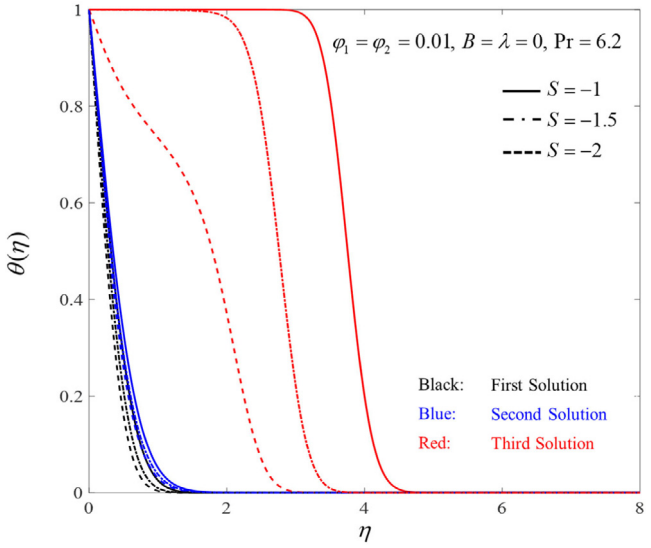

Fig. 7. Temperature profiles $\theta(\eta)$ vs S.

surface ($B = 0.2$) contributes to the enhancement of $\mathrm{Re}_r^{-1/2} Nu_r$ on all solutions. However, the different behaviors are noticed for $\mathrm{Re}_r^{1/2} C_f$ and $\mathrm{Re}_r^{1/2} C_g$. From the physical point of view, at the revolving disk, wall suction causes increasing torque and drag force and lead to the enhancement in the friction factor on the surface. This behavior is shown by the third solution. However, reverse trends are observed for the first and the second solutions. For future reference, the respective numerical values of $\mathrm{Re}_r^{1/2} C_f$, $\mathrm{Re}_r^{1/2} C_g$ and $\mathrm{Re}_r^{-1/2} Nu_r$ for different S when $\varphi_1 = \varphi_2 = 0.01$, $\lambda = B = 0$ and $\mathrm{Pr} = 6.2$ are presented in Table 5.

The soundness of the multiple solutions accomplished is supported with the results of the radial $f'(\eta)$ and azimuthal $g(\eta)$ velocities, as well as the temperature $\theta(\eta)$ profiles as presented in Figs. 5–7. From those figures, the triple distributions exist for fixed values of pertinent parameters where the boundary layer thickness on the third solution is larger than others. The distributions show that the outputs satisfy the far-field boundary conditions asymptotically. For the fixed values of parameters ($\varphi_1 = \varphi_2 = 0.01$, $\lambda = B = 0$, and $\mathrm{Pr} = 6.2$), the boundary layer thickness of the radial $f'(\eta)$ and the azimuthal $g(\eta)$ velocities becomes thinner for stronger deceleration ($S < 0$). The velocities $f'(\eta)$ and $g(\eta)$ on the first solution increase and then decrease to zero. Besides, the velocity of $f'(\eta)$ on the first and the second solutions encounters a positive overshoot and the velocity of the fluid close to the disk is elevated due to strong deceleration. However, there exist reversal flows in $f'(\eta)$ and $g(\eta)$ on the second and the third solutions. Also, the velocity of $f'(\eta)$ and $g(\eta)$ near the disk on the second solution decreases, while the third solution increases as the deceleration strength become higher ($S = -1, -1.5, -2$). On the other hand, the temperature profiles $\theta(\eta)$ on all solutions show the same characteristic where the temperature $\theta(\eta)$ reduces for $S < 0$.

5. Conclusion

A mathematical analysis of the unsteady flow over a rotating disk in a hybrid nanofluid with the suction and the deceleration effects are established. The validity of the mathematical model is demonstrated for the limiting cases by comparing the results with previously published data. The findings are as follows:

- Greater values of the skin friction coefficients $\mathrm{Re}_r^{1/2} C_f$ and $\mathrm{Re}_r^{1/2} C_g$ on the first and third solutions are observed, but

Table 5
Values of $\mathrm{Re}_r^{1/2}C_f$, $\mathrm{Re}_r^{1/2}C_g$ and $\mathrm{Re}_r^{-1/2}Nu_r$ for different S when $\varphi_1 = \varphi_2 = 0.01$, $\lambda = B = 0$ and $\mathrm{Pr} = 6.2$.

Physical quantities	$\mathrm{Re}_r^{1/2}C_f$	$\mathrm{Re}_r^{1/2}C_g$	$\mathrm{Re}_r^{-1/2}Nu_r$
S	First solution		
−1	0.777529	−0.255554	1.769323
−1.5	0.891881	−0.045203	2.056213
−2	1.006233	0.167414	2.307348
−2.5	1.120439	0.381764	2.533316
−3	1.234438	0.597490	2.740352
S	Second solution		
−1	0.520803	−0.089886	1.628050
−1.5	0.312136	0.097533	1.809032
−2	−0.010675	−0.032191	1.951210
−2.5	−0.248856	−0.395705	2.139540
−3	−0.409455	−0.726846	2.343066
S	Third solution		
−1	−1.307270	−0.676955	0.000000
−1.5	−1.096882	−0.243161	0.001025
−2	−1.060936	0.276207	0.418375
−2.5	−0.826266	1.171284	1.685648
−3	−0.554995	2.540384	2.187704

they are reduced on the second solution for the stronger deceleration.

- The values of $\mathrm{Re}_r^{1/2}C_f$ and $\mathrm{Re}_r^{1/2}C_g$ on the third solution are enhanced in the presence of suction. However, reverse trends are observed for their first and second solutions.
- The imposition of suction on the surface and stronger deceleration strength contributes to the enhancement of $\mathrm{Re}_r^{-1/2}Nu_r$ on all solutions.
- The multiple solutions exist for fixed values of pertinent parameters where the profiles satisfy the far-field boundary conditions asymptotically.
- The existence of multiple solutions is verifiable in certain operating parameters. From the temporal stability analysis, the first and the second solutions are significantly realizable and stable, while the third solution is unstable, over time.

Declaration of competing interest

The authors declare that they have no known competing financial interests or personal relationships that could have appeared to influence the work reported in this paper.

Acknowledgments

The financial supports received from the Universiti Kebangsaan Malaysia (Project Code: DIP-2020-001) and the Universiti Teknikal Malaysia Melaka are gratefully acknowledged.

References

[1] M. Favre-Marinet, S. Tardu, Convective Heat Transfer, ISTE Ltd, London, 2009.
[2] S.U.S. Choi, J.A. Eastman, Enhancing thermal conductivity of fluids with nanoparticles, in: Proc. 1995 ASME Int. Mech. Eng. Congr. Expo. FED 231/MD, Vol. 66, 1995, pp. 99–105.
[3] K. Khanafer, K. Vafai, M. Lightstone, Buoyancy-driven heat transfer enhancement in a two-dimensional enclosure utilizing nanofluids, Int. J. Heat Mass Transfer 46 (2003) 3639–3653.
[4] R.K. Tiwari, M.K. Das, Heat transfer augmentation in a two-sided lid-driven differentially heated square cavity utilizing nanofluids, Int. J. Heat Mass Transfer 50 (2007) 2002–2018.
[5] H.F. Oztop, E. Abu-Nada, Numerical study of natural convection in partially heated rectangular enclosures filled with nanofluids, Int. J. Heat Fluid Flow. 29 (2008) 1326–1336.
[6] M.A.A. Hamad, Analytical solution of natural convection flow of a nanofluid over a linearly stretching sheet in the presence of magnetic field, Int. Commun. Heat Mass Transf. 38 (2011) 487–492.
[7] T. Hayat, M. Rashid, A. Alsaedi, MHD convective flow of magnetite-Fe3o4 nanoparticles by curved stretching sheet, Results Phys. 7 (2017) 3107–3115.
[8] N.V. Ganesh, A.K.A. Hakeem, B. Ganga, Darcy–Forchheimer flow of hydromagnetic nanofluid over a stretching/shrinking sheet in a thermally stratified porous medium with second order slip, viscous and Ohmic dissipations effects, Ain Shams Eng. J. 9 (2018) 939–951.
[9] R. Jusoh, R. Nazar, I. Pop, Magnetohydrodynamic boundary layer flow and heat transfer of nanofluids past a bidirectional exponential permeable stretching/shrinking sheet with viscous dissipation effect, J. Heat Transfer. 141 (2019) 012406.
[10] P.K. Kameswaran, M. Narayana, P. Sibanda, P.V.S.N. Murthy, Hydromagnetic nanofluid flow due to a stretching or shrinking sheet with viscous dissipation and chemical reaction effects, Int. J. Heat Mass Transfer 55 (2012) 7587–7595.
[11] O.D. Makinde, I.L. Animasaun, Bioconvection in MHD nanofluid flow with nonlinear thermal radiation and quartic autocatalysis chemical reaction past an upper surface of a paraboloid of revolution, Int. J. Therm. Sci. 109 (2016) 159–171.
[12] U. Khan, A. Zaib, I. Khan, K.S. Nisar, Activation energy on MHD flow of titanium alloy (Ti6Al4V) nanoparticle along with a cross flow and streamwise direction with binary chemical reaction and non-linear radiation: Dual solutions, J. Mater. Res. Technol. 9 (2020) 188–199.
[13] K. Das, N. Acharya, P.K. Kundu, The onset of nanofluid flow past a convectively heated shrinking sheet in presence of heat source/sink: A Lie group approach, Appl. Therm. Eng. 103 (2016) 38–46.
[14] A. Jamaludin, R. Nazar, I. Pop, Mixed convection stagnation-point flow of a nanofluid past a permeable stretching/shrinking sheet in the presence of thermal radiation and heat source/sink, Energies 12 (2019) 788.
[15] D. Pal, G. Mandal, K. Vajravalu, Soret and Dufour effects on MHD convective-radiative heat and mass transfer of nanofluids over a vertical non-linear stretching/shrinking sheet, Appl. Math. Comput. 287–288 (2016) 184–200.
[16] I. Waini, A. Ishak, I. Pop, Dufour and Soret effects on Al2o3-water nanofluid flow over a moving thin needle: Tiwari and das model, Int. J. Numer. Methods Heat Fluid Flow. 31 (2021) 766–782.
[17] C. Sulochana, S.P. Samrat, N. Sandeep, Boundary layer analysis of an incessant moving needle in MHD radiative nanofluid with joule heating, Int. J. Mech. Sci. 128–129 (2017) 326–331.
[18] X.H. Zhang, A. Abidi, A.E.S. Ahmed, M.R. Khan, M.A. El-Shorbagy, M. Shutaywi, A. Issakhov, A.M. Galal, MHD stagnation point flow of nanofluid over a curved stretching/shrinking surface subject to the influence of Joule heating and convective condition, Case Stud. Therm. Eng. 26 (2021) 101184.
[19] R. Ellahi, A. Zeeshan, F. Hussain, T. Abbas, Study of shiny film coating on multi-fluid flows of a rotating disk suspended with nano-sized silver and gold particles: A comparative analysis, Coatings 8 (2018) 422.
[20] R. Ellahi, S.M. Sait, N. Shehzad, Z. Ayaz, A hybrid investigation on numerical and analytical solutions of electro-magnetohydrodynamics flow of nanofluid through porous media with entropy generation, Int. J. Numer. Methods Heat Fluid Flow. 30 (2020) 834–854.
[21] M. Turkyilmazoglu, Natural convective flow of nanofluids past a radiative and impulsive vertical plate, J. Aerosp. Eng. 29 (2016) 04016049.
[22] M. Turkyilmazoglu, Nanoliquid film flow due to a moving substrate and heat transfer, Eur. Phys. J. Plus. 135 (2020) 781.
[23] N.A.C. Sidik, I.M. Adamu, M.M. Jamil, G.H.R. Kefayati, R. Mamat, G. Najafi, Recent progress on hybrid nanofluids in heat transfer applications: A comprehensive review, Int. Commun. Heat Mass Transf. 78 (2016) 68–79.
[24] R. Turcu, A. Darabont, A. Nan, N. Aldea, D. Macovei, D. Bica, L. Vekas, O. Pana, M.L. Soran, A.A. Koos, L.P. Biro, New polypyrrole-multiwall carbon nanotubes hybrid materials, J. Optoelectron. Adv. Mater. 8 (2006) 643–647.
[25] S. Jana, A. Salehi-Khojin, W.H. Zhong, Enhancement of fluid thermal conductivity by the addition of single and hybrid nano-additives, Thermochim. Acta. 462 (2007) 45–55.
[26] S. Suresh, K.P. Venkitaraj, P. Selvakumar, M. Chandrasekar, Synthesis of Al2o3-cu/water hybrid nanofluids using two step method and its thermo physical properties, Colloids Surf. A Physicochem. Eng. Asp. 388 (2011) 41–48.
[27] S.K. Singh, J. Sarkar, Energy, exergy and economic assessments of shell and tube condenser using hybrid nanofluid as coolant, Int. Commun. Heat Mass Transf. 98 (2018) 41–48.
[28] K. Farhana, K. Kadirgama, M.M. Rahman, M.M. Noor, D. Ramasamy, M. Samykano, G. Najafi, N.A.C. Sidik, F. Tarlochan, Significance of alumina in nanofluid technology: An overview, J. Therm. Anal. Calorim. 138 (2019) 1107–1126.
[29] B. Takabi, S. Salehi, Augmentation of the heat transfer performance of a sinusoidal corrugated enclosure by employing hybrid nanofluid, Adv. Mech. Eng. 6 (2014) 147059.

[30] A. Jamaludin, K. Naganthran, R. Nazar, I. Pop, MHD mixed convection stagnation-point flow of Cu-Al2o3/water hybrid nanofluid over a permeable stretching/shrinking surface with heat source/sink, Eur. J. Mech. B/Fluids 84 (2020) 71–80.
[31] U. Khan, I. Waini, A. Ishak, I. Pop, Unsteady hybrid nanofluid flow over a radially permeable shrinking/stretching surface, J. Mol. Liq. 331 (2021) 115752.
[32] N.S. Khashi'ie, N.M. Arifin, N. Wahi, I. Pop, R. Nazar, E.H. Hafidzuddin, Thermal marangoni flow past a permeable stretching/shrinking sheet in a hybrid Cu-Al2o3/water nanofluid, Sains Malays. 49 (2020) 211–222.
[33] N.A. Zainal, R. Nazar, K. Naganthran, I. Pop, MHD flow and heat transfer of hybrid nanofluid over a permeable moving surface in the presence of thermal radiation, Int. J. Numer. Methods Heat Fluid Flow. 31 (2021) 858–879.
[34] I. Waini, A. Ishak, I. Pop, Hiemenz flow over a shrinking sheet in a hybrid nanofluid, Results Phys. 19 (2020) 103351.
[35] I. Waini, A. Ishak, I. Pop, Flow and heat transfer of a hybrid nanofluid past a permeable moving surface, Chinese J. Phys. 66 (2020) 606–619.
[36] I. Waini, A. Ishak, I. Pop, Symmetrical solutions of hybrid nanofluid stagnation-point flow in a porous medium, Int. Commun. Heat Mass Transf. 130 (2022) 105804.
[37] M. Hassan, M. Marin, R. Ellahi, S.Z. Alamri, Exploration of convecti ve heat transfer and flow characteristics synthesis by cu-Ag/Water hybrid-nanofluids, Heat Transf. Res. 49 (2018) 1837–1848.
[38] A. Riaz, R. Ellahi, S.M. Sait, Role of hybrid nanoparticles in thermal performance of peristaltic flow of Eyring–Powell fluid model, J. Therm. Anal. Calorim. 143 (2021) 1021–1035.
[39] J. Sarkar, P. Ghosh, A. Adil, A review on hybrid nanofluids: Recent research, development and applications, Renew. Sustain. Energy Rev. 43 (2015) 164–177.
[40] J.A.R. Babu, K.K. Kumar, S.S. Rao, State-of-art review on hybrid nanofluids, Renew. Sustain. Energy Rev. 77 (2017) 551–565.
[41] G. Huminic, A. Huminic, Entropy generation of nanofluid and hybrid nanofluid flow in thermal systems: A review, J. Mol. Liq. 302 (2020) 112533.
[42] L. Yang, W. Ji, M. Mao, J. Huang, An updated review on the properties, fabrication and application of hybrid-nanofluids along with their environmental effects, J. Clean. Prod. 257 (2020) 120408.
[43] T. Von Kármán, Über laminare und turbulente Reibung, Zeitschrift Für Angew. Math. Und Mech. (1921) 233–252.
[44] T. Fang, Flow over a stretchable disk, Phys. Fluids. 19 (2007) 128105.
[45] T. Fang, J. Zhang, Flow between two stretchable disks - An exact solution of the Navier–Stokes equations, Int. Commun. Heat Mass Transf. 35 (2008) 892–895.
[46] M. Turkyilmazoglu, MHD fluid flow and heat transfer due to a stretching rotating disk, Int. J. Therm. Sci. 51 (2012) 195–201.
[47] M. Turkyilmazoglu, Heat and mass transfer on the unsteady magnetohydrodynamic flow due to a porous rotating disk subject to a uniform outer radial flow, J. Heat Transfer. 132 (2010) 061703.
[48] M. Turkyilmazoglu, Unsteady flow over a decelerating rotating sphere, Phys. Fluids. 30 (2018) 033601.
[49] L.T. Watson, C.Y. Wang, Deceleration of a rotating disk in a viscous fluid, Phys. Fluids. 22 (1979) 2267–2279.
[50] L.T. Watson, K.K. Sankara, L.C. Mounfield, Deceleration of a porous rotating disk in a viscous fluid, Internat. J. Engrg. Sci. 23 (1985) 131–137.
[51] T. Fang, H. Tao, Unsteady viscous flow over a rotating stretchable disk with deceleration, Commun. Nonlinear Sci. Numer. Simul. 17 (2012) 5064–5072.
[52] K. Naganthran, M. Mustafa, A. Mushtaq, R. Nazar, Dual solutions for fluid flow over a stretching/shrinking rotating disk subject to variable fluid properties, Phys. A Stat. Mech. Appl. 556 (2020) 124773.
[53] G.M. Sarkar, B. Sahoo, On dual solutions of the unsteady MHD flow on a stretchable rotating disk with heat transfer and a linear temporal stability analysis, Eur. J. Mech. B/Fluids. 85 (2021) 149–157.
[54] T. Rafiq, M. Mustafa, Computational analysis of unsteady swirling flow around a decelerating rotating porous disk in nanofluid, Arab. J. Sci. Eng. 45 (2020) 1143–1154.
[55] J.H. Merkin, On dual solutions occurring in mixed convection in a porous medium, J. Eng. Math. 20 (1986) 171–179.
[56] P.D. Weidman, D.G. Kubitschek, A.M.J. Davis, The effect of transpiration on self-similar boundary layer flow over moving surfaces, Internat. J. Engrg. Sci. 44 (2006) 730–737.
[57] S.D. Harris, D.B. Ingham, I. Pop, Mixed convection boundary-layer flow near the stagnation point on a vertical surface in a porous medium: Brinkman model with slip, Transp. Porous Media. 77 (2009) 267–285.
[58] L.F. Shampine, I. Gladwell, S. Thompson, Solving ODEs with MATLAB, Cambridge University Press, Cambridge, 2003.
[59] L.F. Shampine, J. Kierzenka, M. Reichelt, Solving boundary value problems for ordinary differential equations in MATLAB with bvp4c, in: Tutor. Notes, 2000, pp. 1–27.